6.0 POTENTIAL EARTHQUAKE GROUND MOTIONS

The potential for strong ground shaking at the site due to earthquakes is assessed based on a probabilistic seismic hazard analysis (PSHA). Section 6.1 describes the PSHA methodology used in this study. The characteristics of earthquake sources (active faults and seismic source areas) used in the hazard analysis are described in Section 6.2 and the results are presented in Section 6.3. Section 6.4 compares the PSHA results to ground motion estimates based on a deterministic analysis.

The design basis ground motions for the proposed PFSF site were arrived at using a deterministic approach, consistent with Part 72.102 and 10 CFR Part 100 for nuclear power plants. A deterministic approach assumes that the maximum credible earthquake on all capable sources will occur at the closest approach to the site. The controlling source results in the largest ground motions at the site and determines the SSE ground motions. The deterministic design basis ground motions at the proposed PFSF site were presented in the SAR (Section 2.6.2). Deterministic approaches do not incorporate any information related to the frequency of earthquake occurrence, nor do they allow for the explicit inclusion of uncertainties in the location, size, or ground motions associated with earthquakes. For these reasons, Part 100 has been revised (Part 100.23) to allow for probabilistic methodologies to be used to arrive at design basis ground motions. Part 72 has not yet been revised, but the rulemaking plan (SECY-98-126) indicates that probabilistic approaches should likewise be used for dry cask storage installations. Therefore, we have conducted a probabilistic seismic hazard analysis that incorporates the findings of the field studies and associated uncertainties. To evaluate the potential for fault displacement at the site, a probabilistic fault displacement analysis was also conducted (Section 7).

6.1 PSHA METHODOLOGY

6.1.1 Probability Level of Interest

Probabilistic seismic hazard analyses result in "hazard curves" that express the probability (or annual frequency) of exceeding various levels of ground motion. Lower probability levels are associated with progressively higher levels of ground motion. As such, the probability levels express the degree of conservatism in the ground motions to be used for design. The NRC recommends that a risk-informed graded approach to seismic design be used that takes into account the consequences of the possible failure of a system in arriving at an appropriate probability level. The NRC staff recognizes the value of this approach in its evaluation of the request for exemption to Part 72.102(f)(1) Seismic Design Requirement for Three Mile Island

Unit 2 Independent Spent Fuel Storage Installation (SECY-98-071), and in its Rulemaking Plan for revision to Part 72 (SECY-98-126). The Commission stated that "...ISFSI's which do not involve massive structures, such as dry storage casks and canisters, the required design earthquake will be determined on a case-by-case basis..." (45 FR 74697 [1980]). In its Rulemaking Plan, it is stated that the "NRC staff believed that a major seismic event at an ISFSI storing spent fuel in dry casks or canisters would most likely have minor radiological consequences compared with a major seismic event at an NPP, spent fuel pool, or single massive storage structure" (SECY-98-126). The NRC, therefore, recommends that a probabilistic approach be taken and that the probability levels appropriate to the design of a dry cask storage system should be higher (i.e., ground motions lower) than those for a nuclear power plant.

Until the Part 72 rulemaking is completed, there is only indirect guidance from the Staff regarding the appropriate probability level for seismic design. In the exemption to Part 72.102, the seismic requirement (design earthquake or DE) for the TMI-2 ISFSI was 0.35g peak ground acceleration, corresponding to a ~5 x 10^{-4} per year probability level (or ~2,000 year return period). The deterministic SSE at the INEL site was assessed to be 0.56g. In arriving at their decision, the Staff considered the appropriateness of a probabilistic methodology and a risk-informed graded approach. They noted that such a graded approach, which expresses the relative risk posed by the ISFSI, has been developed in DOE Standard 1020 "Natural Phenomena Hazards Design and Evaluation Criteria for Department of Energy Facilities." The standard takes a graded approach to design critical facilities, requiring facilities with greater accident consequences to use higher design requirements for phenomena such as earthquakes and tornadoes. They conclude, "Dry spent fuel storage facilities such as the TMI-2 ISFSI are PC 3 and must have a design earthquake equal to the mean ground motion with a 2,000-year return period. Considering the minor radiological consequences from a canister failure, and the lack of a credible mechanism to cause a failure, the staff finds that the DOE approach of using the 2,000-year return period mean ground motion as the design earthquake for dry storage facilities is adequately conservative."

The staff also note that the 10 CFR Part 60 Design Basis Event rulemaking also adopts a graded approach. In this approach, a design basis event is based on a probabilistic, risk-graded methodology. For seismic events, the staff has accepted DOE's two-tiered approach toward designing Part 60 SSCs. Those SSCs with potential failure consequences less than the public dose limit of 10 CFR 20.1302(a)(1), 1 mSv (100 mrem), must withstand the 1,000-year return period mean ground motion. Analysis of the consequences associated with a cask failure at the

PFSF are less than the 100 mrem dose limit, thus suggesting that the 1,000-year return period is appropriate.

Based on the above arguments for a risk-informed graded approach, we conclude that an appropriate design probability level for the PFSF site is 5 x 10^{-4} (2,000-year return period). The design basis ground motions presented in the SAR were based on a deterministic approach and did not incorporate the uncertainties associated with seismic sources, recurrence, or attenuation relationships. The PSHA presented herein does include these uncertainties explicitly, including the findings of the fault studies. The deterministically defined design basis ground motions are compared with the 2,000-year ground motions derived from the probabilistic approach, and are shown to be conservative relative to this criterion.

6.1.2 Implementation of PSHA Methodology in This Study

Basic Model

The methodology used for the probabilistic assessment of ground motion hazard at the Skull Valley site follows that outlined for the Yucca Mountain project as described in USDOE (1997) and CRWMS M&O (1998). The methodology for a PSHA was first proposed by Cornell (1968, 1971). The basic components of the PSHA for ground motion hazard are shown schematically on Figure 6-1. The components are as follows.

1. The sources of potentially damaging future earthquakes are identified. The types of sources typically identified are specific geologic structures, such as faults, and areal source zones representing tectonic provinces or zones of seismicity.

2. The frequency of earthquake occurrence in each source is assessed. This includes an evaluation of the maximum event that a source can produce. The probability distribution of distance from individual earthquakes to the site is also defined by specifying the appropriate spatial distribution model for earthquake location on the seismic source.

3. Appropriate ground motion attenuation models are selected for estimating site ground motions from each source. The estimates include both the expected levels of ground motion and the variation about the expected value that any recording may exhibit.

4. Using the probabilistic models developed in steps (2) and (3), a relationship between ground motion level and probability (frequency) at which it is exceeded is developed, defining a *hazard curve*. Specific ground motion levels for design can then be chosen by selecting an appropriate probability level.

The mathematical formulation used for PSHA typically assumes that the occurrence of damaging earthquakes can be represented as a Poisson process. Under this assumption, the probability that a ground motion parameter, Z, will exceed a specified value, z, in time period t is given by:

$$P(Z > z | t) = 1 - e^{-\nu(z) \cdot t} \leq \nu(z) \cdot t \qquad \textbf{(6-1)}$$

where $\nu(z)$ is the average frequency during time period t at which the level of ground motion parameter Z exceeds value z at the site from all earthquakes on all sources in the region. The inequality at the right of Equation **(6-1)** is valid regardless of the probability model for earthquake occurrence, and $\nu(z) \cong t$ gives an accurate and slightly conservative estimate of $P(Z > z)$ for probabilities of 0.1 or less, if $\nu(z)$ is the appropriate average value for time period t.

The frequency of exceedance, $\nu(z)$, is a function of the frequency of earthquake occurrence, the randomness of size and location of future earthquakes, and the randomness in the level of ground motion they may produce at the site. It is computed by the expression:

$$\nu(z) = \sum_n \alpha_n(m^0) \int_{m^0}^{m^u} f(m) \left[\int_0^\infty f(r|m) \cdot P(Z > z|m,r) \cdot dr \right] \cdot dm \qquad \textbf{(6-2)}$$

where $\alpha_n(m^0)$ is the frequency of earthquakes on source n above a minimum magnitude of engineering significance, m^0; $f(m)$ is the probability density of earthquake size between m^0 and a maximum earthquake the source can produce, m^u; $f(r \mid m)$ is the probability density function for distance to an earthquake of magnitude m occurring on source n; and $P(Z>z \mid m,r)$ is the probability that, given an earthquake of magnitude m at distance r from the site, the peak ground motion will exceed level z.

Section 6.2 describes the implementation of steps (1) and (2) for this project: identification of the seismic sources that may produce earthquakes significant to ground motion hazard at the site, and for each source an assessment of the frequency of earthquake occurrence, $\alpha_n(m^0)$, the maximum earthquake the source can produce, m^u; the distribution of earthquake sizes, $f(m)$, and the spatial distribution of earthquakes on the source. Section 6.3 describes the implementation of step (3): selection of appropriate ground motion models for assessing the probability of exceeding specified ground motion levels as a function of magnitude and distance, $P(Z>z \mid m,r)$. Section 6.4 describes the implementation of step (4), computation of the hazard at the site.

Assessment of Scientific Uncertainty

The PSHA methodology outlined on Figure 6-1 and defined by Equation (6-2) is formulated to represent the randomness inherent in the natural phenomena of earthquake generation and seismic wave propagation. The randomness in a physical process has come to be called *aleatory* uncertainty (SSHAC, 1997). In all assessments of the effects of rare phenomena, one faces uncertainty in selecting the appropriate models and model parameters because the data are limited and/or there are alternative interpretations of the data. This uncertainty in knowledge has come to be called *epistemic* uncertainty (SSHAC, 1997).

The uncertainty assessment was performed using the *logic tree* methodology. The logic tree formulation for seismic hazard analysis (Kulkarni and others, 1984; Coppersmith and Youngs, 1986; Electric Power Research Institute, 1988; National Research Council, 1988) involves setting out the sequence of assessments that must be made in order to perform the analysis and then addressing the uncertainties in each assessment sequentially. Thus, it provides a convenient approach for breaking a large, complex assessment into a sequence of smaller, simpler components that can be addressed more easily.

Figure 6-2 shows an example of a logic tree. The logic tree is composed of a series of nodes and branches. Each node represents a state of nature or an input parameter that must be assessed to perform the analysis. Each branch leading from a node represents one possible alternative interpretation of the state of nature or parameter being evaluated. If the variable in question is continuous, it can be discretized at a suitable increment. The branches at each node are intended to represent mutually exclusive and collectively exhaustive states of the input parameter. In practice, a sufficient number of branches are placed at a given node to represent the evaluator's uncertainty in estimating the parameter.

Probabilities are assigned to each branch that represent the expert's evaluation that the branch represents the correct value or state of the input parameter. These probabilities are conditional on the assumption that all the branches leading to that node represent the true state of the preceding parameters. Because they are conditional probabilities for a mutually exclusive and collectively exhaustive set of values, the sum of the conditional probabilities at each node is unity. The probabilities are based on scientific evaluations because the available data are too limited to allow for objective statistical analysis, and because scientific evaluation is needed to weigh alternative interpretations of the available data. The logic tree simplifies these assessments, because the uncertainty in each parameter is considered individually, independent of prior evaluations. The nodes of the logic tree are sequenced to express conditional aspects or dependencies among the parameters and to provide a logical progression of evaluations from general to specific in characterizing the input parameters for PSHA.

The probabilities (relative weights) assigned to the branches at a node of the logic tree represent one of two types of probability assessments. For the first type, the branches at a node define the range of parameter values; the associated weights define the probability distribution for the parameter. For example, estimates of the slip rate on a fault are uncertain because of uncertainties in the amount of displacement of a particular geologic unit across the fault and the age of the unit. The probability distribution for a parameter value may be characterized in several ways: as a discrete distribution defined by a preferred value and a range of discrete higher and lower values; a cumulative distribution based on scientific evaluations; or by a mean estimate and an uncertainty estimate similar to a normal or log-normal statistical distribution. Examples of these means of characterization are given below. Continuous distributions can be discretized to form logic tree branches following a number of approaches. Keefer and Bodily (1983) showed that most distributions can be represented reliably by three values: the median estimate (50^{th} percentile), assigned a weight of 0.63, and a higher and lower value, each given weights of 0.185, which represent the 5^{th} and 95^{th} percentiles (± 1.645 standard deviations for a normal distribution). They list other discretization schemes for more points. Another four-point representation of a normal distribution is described in EPRI (1993, Chapter 9). Miller and Rice (1983) present a number of discrete approximations to subjectively defined, continuous cumulative distributions.

In some instances, the uncertainty in assessing parameters can be estimated using formal statistical techniques. In these cases, continuous parameter distributions developed from statistical estimation procedures can be discretized for use in a logic tree formulation.

A second type of probability assessment, to which logic trees are particularly well suited, is indicating a relative preference for, or degree of belief in, alternative hypotheses. For example, the sense of slip on a fault may be uncertain–two alternatives might be strike-slip or reverse-slip. Based on the pertinent data, a relative preference for these alternatives can be expressed by weights in the logic tree. A very strong preference (i.e., the data strongly support one interpretation over the other) for one alternative over the other usually is represented by weights such as 0.9 and 0.1. If there is no preference (i.e., the data equally support either alternative) for either hypothesis, they are assigned equal weights (0.5 and 0.5 for two hypotheses). Increasing the weight assigned to one alternative from 0.5 to 0.9 (or more) reflects increasing support in the data for that alternative. Because the relative weights ultimately are the result of scientific evaluations based on available information, it is important to document the data and interpretations that led to the characterization of parameter values and their relative weights so that the process can be reviewed by others.

The example logic tree shown on Figure 6-2 characterizes the uncertainty in assessing the magnitude of paleoearthquakes that have occurred on a fault on the basis of dip-slip offsets observed in a trench placed across the fault. (Such assessments may be one means of characterizing the maximum magnitude for a seismic source.) There may be multiple sources of uncertainty in the assessment. Stratigraphic relationships in the trench walls may be somewhat ambiguous so that the amount of dip-slip displacement can be estimated only within a factor of two (e.g., 1.0 to 2.0 meters). One may also be uncertain about the existence of a significant component of lateral slip, which would indicate whether the fault is primarily a normal fault or an oblique-normal fault having a ratio of strike slip to dip slip in the range of 1:1 to 1.5:1. In addition, there is the uncertainty in whether the observed slip is more representative of the maximum slip during the paleoearthquake or the average slip.

The logic tree shown at the left of Figure 6-2 captures these uncertainties. The required interpretations in the logic tree usually are ordered from general to specific. If one interpretation depends on the state of another unknown, then it is placed to the right of that assessment in the logic tree. In this example, the total amount of fault offset is dependent on whether the fault is a normal fault or an oblique-normal fault. In addition, the evaluation of whether the observed displacement is representative of the maximum or the average displacement may also depend on the style of faulting. The trench may have been placed in an area where the fault scarp was most pronounced, indicative of maximum vertical displacement. However, this may not be the area of maximum slip if the fault is oblique-normal. Because these two interpretations are made more easily given knowledge of the style of faulting, the node for interpretations of the style of faulting is placed first (to the left) in the logic tree. The order of the interpretations is dictated primarily by convenience in dealing with dependencies in the characterization. After the logic tree is constructed, the order of the nodes can be changed.

For the example shown on Figure 6-2, the evaluation of the assessor is that the interpretation of normal faulting is preferred slightly (0.6) to the interpretation of oblique-normal faulting (0.4). In actual interpretations, the assessor documents the reasons for this evaluation.

The next level of characterization in the example addresses the amount of displacement. The stratigraphic relationships indicate from 1.0 to 2.0 of offset. The interpretation of these data may favor displacements in the range of 1.0 to 1.5 but allow for as much as 2.0 meters. Thus, if the fault is a normal fault, the distribution for the observed offset may be specified by three discrete values: 1.0, 1.5, and 2.0 m. The probabilities (relative weights) assigned to these values are 0.4, 0.4, and 0.2, respectively, reflecting that the data more strongly support displacements of 1.0 to 1.5 m.

If the fault is considered an oblique-normal fault, then the observed offsets must be increased to account for unmeasured strike-slip offset to obtain the net slip on the fault plane. The factor of increase is 1.4 for a 1:1 strike-sip/dip-slip ratio, and 1.6 for a 1.5:1 strike-sip/dip-slip ratio. In this example, it is considered twice as likely that the strike-slip to dip-slip ratio is closer to 1:1 than to 1.5:1. Thus the factors are given relative weights of 0.67 and 0.33. The evaluation of the strike-slip to dip-slip ratio is added to the logic tree after the branch for oblique-normal faulting. The evaluation is unnecessary along the normal faulting branch. There the distributions for the amount of net slip are assumed to be equal to those developed for normal faulting multiplied by the appropriate factor.

The final evaluation is whether the observed offsets represent maximum displacements or average displacements. This evaluation is important because separate empirical relationships between magnitude and fault offset are given for maximum and average displacement (e.g., Wells and Coppersmith, 1994). This evaluation is made conditionally on which sense of slip is assumed to be correct--that is, the probability that the observed offset is a maximum given normal faulting is a separate evaluation from the probability that it is a maximum displacement given oblique-normal faulting, and the two probabilities do not have to be equal. In the example the data strongly support the interpretation that the observed displacements represent maximum (0.8) rather than average (0.2) values if the style of faulting is deemed normal. If the fault is considered oblique-normal, then the maximum and average displacement is considered to be equivocal, and the two alternatives are given equal weight.

Each end branch on the right-hand side of the logic tree shown at the left of Figure 6-2 specifies one estimate for the magnitude of the paleoearthquake. The magnitude estimate is obtained using the appropriate empirical relationship between fault displacement (either average or maximum) and moment magnitude given by Wells and Coppersmith (1994). Their relationships for normal faulting earthquakes were used for the normal style of faulting; their relationships for strike-slip faulting were used for the oblique-normal style of faulting. The resulting magnitudes are listed along the right side of the logic tree. The probability that the magnitude for the paleoearthquake will take on any particular value is equal to the joint probability of the set of parameters (branches) leading to that assessment. These probabilities are given in parentheses next to the magnitude assessments. The characterization in the logic tree specifies a discrete distribution for the magnitude of the paleoearthquake. This distribution is shown at the right of Figure 6-2 in discrete density and cumulative forms.

The process illustrated above for characterizing the magnitude of paleoearthquakes was used to quantitatively express the uncertainty in the seismic source and ground motion attenuation characterization for ground shaking hazard. These assessments are described in Sections 6.2 and 6.3.

6.2 SEISMIC SOURCE CHARACTERIZATION

Seismic sources include all structures that have some potential for causing strong ground shaking at the PFSF. The seismic source model developed for this study includes two types of sources: (1) *fault-specific sources,* which include mapped late Quaternary faults within about 100 km of the site, and (2) *seismic source zones* to account for seismicity that cannot be attributed to fault-specific sources included in the model (Figure 6-1). Different approaches are used to characterize these two types of sources as discussed below.

6.2.1 Fault Sources

Active faults within 100 km of the proposed PFSF site (Plate 7) are listed in Table 6-1. These faults, excepting the recently identified East and West faults, are described in the previous SAR submittal (SWEC, 1997). Faults from this group that are included as fault sources in the seismic source model for this analysis are judged to be capable of generating magnitude 5 or larger earthquakes and, based on published reports, are inferred to have had multiple late Quaternary displacements. Several faults that are known or suspected to have had Quaternary displacement, but are not reported to exhibit evidence of late Quaternary displacement, are not included as fault-specific seismic sources. The rate of slip on these faults is too low to have a significant effect on the ground motion hazard at the site. Relatively short (<10 km) faults that lie at distances greater than 25 km also would not contribute significantly. Earthquakes that occur on Quaternary or suspected Quaternary faults that are not included as fault sources are modeled as part of the seismic source zones.

Seismic sources that might make a significant contribution to the seismic hazard at the PFSF (either because they have a relatively high rate of activity and/or because they are close to the site) are characterized in greater detail than sources far from the site. These include the Stansbury fault, the East Cedar Mountains fault, and the mid-valley faults (East fault, West fault, and postulated Springline fault) (Plates 6 and 7). Regional structural cross sections and alternative structural models for these faults as presented in Section 2.0 and paleoseismic data discussed in Section 5 provide the basis for our characterization of these local fault sources.

6.2.1.1 Fault Source Characterization Parameters

The logic tree used to characterize fault sources is shown on Figure 6-3. The key parameters used to define the seismic hazard potential of significant crustal fault seismic sources are: total fault length and plan view geometry; probability of activity; maximum magnitude; and recurrence parameters. The assessment of these parameters are based on consideration of the maximum rupture length of faults, seismogenic crustal thickness and downdip geometry that can be used to estimate downdip width, and slip rates. The range of values and relative weights applied for each of these parameters in the probabilistic hazard analysis are provided in Table 6-2.

Total Fault Length and Plan View Geometry

Discontinuous faults are generalized as a single continuous trace consisting of one or more straight line segments, so that the average source-to-site distance and total length of the modeled fault are consistent with the mapped fault.

Probability of Activity

The assessment of activity for crustal faults reflects the judgment of the likelihood that the structure is seismogenic, or active, within the present tectonic regime and will, therefore, localize seismicity above the levels occurring randomly within the regional source zones. Faults for which there is evidence for late Quaternary (approximately the past 780 ka) are assumed to be associated with past seismogenic fault displacements [probability of activity = 1.0]. Faults for which there is questionable evidence for late Quaternary activity or that have limited downdip extent (i.e., may not extend to seismogenic depth) are assigned a probability of activity of less than 1.0.

Maximum Earthquake Magnitude

The assessment of maximum magnitude for fault sources is based on empirical relationships between magnitude and rupture length, magnitude and rupture area, magnitude and single event displacement (if data are available for the maximum and/or average displacement per event) (Wells and Coppersmith, 1994); the relationship of Anderson and others (1996) between magnitude, rupture length, and slip rate; and the relationship between magnitude, rupture length, and maximum displacement (Mason, 1996). Where the appropriate data are available, all of these techniques were used. The individual techniques were assigned relative weights that reflect the combined weights of expert panel members who characterized the seismic source parameters for the Yucca Mountain PSHA (CRWMS, 1998). The weights assigned to the various empirical methods varied among the different experts. However, when viewed collectively, the judgements of the eighteen panel members indicate that the most weight is given to relationships based on rupture length and/or rupture area. These two methods received about equal weight with the rupture length relationship being favored slightly over the rupture area relationship. The relationship based on rupture length plus slip rate received the lowest weight. Assigned weights for this method ranged from 0 to 0.4 with the collective weight being less than or about equal to 0.1. Relationships based on displacement (either maximum displacement or average displacement) were considered less stable than those based an rupture length and area and also were assigned a low weight that was only a little higher than the weight assigned to the relationship based on rupture length plus slip rate. If displacement data are available, the relative weights assigned to the methods for estimating maximum magnitude are: magnitude versus rupture length [0.4]; magnitude versus rupture area [0.35]; magnitude versus displacement [0.15]; magnitude versus rupture length and maximum displacement [0.05]; and magnitude versus rupture length and slip rate [0.05]. When using displacement to estimate magnitude, average displacement is considered to be a more stable indicator of the size of the earthquake than maximum displacement, which only occurs along a very short length of the total rupture. Given the displacement method, the relation based on average displacement is assigned a weight of 0.7 and the one based on maximum displacement is assigned a weight of 0.3. If displacement data are not available, the method relating magnitude to rupture length and slip rate is assigned a weight of 0.1 and the remaining weight is assigned equally between the other methods.

The maximum magnitude distribution includes alternative rupture scenarios as described for each fault source and reflects the postulated maximum rupture dimensions based on combinations of rupture length and width. The maximum rupture length depends on the total fault length and on the length of the longest part of the fault that is expected to rupture during a single event. Various criteria are used to assess possible rupture segmentation scenarios for independent fault sources. Rupture of the total fault length is generally considered; for long faults this option is given relatively low weight especially if paleoseismic data on recency and recurrence suggest multiple rupture segment scenarios are more likely. For short faults, 100 percent of the total fault length commonly is given a probability of 1. Paleoseismic data regarding the timing and dimensions of previous surface ruptures are used where available to delimit rupture segments. Geometric and other geologic constraints also are considered in assigning weights to various possible rupture scenarios. Down-dip width is computed from fault dip, thickness of the seismogenic zone, and limitations imposed by fault geometries where two faults intersect.

Seismicity data indicate that the largest historical earthquakes in the Basin and Range province occurred on 45 to 65 degree dipping normal faults that nucleated at depths of about 15 km (Smith and others, 1985). All the faults included in the seismic source model are high-angle normal faults. We represent the uncertainty in the fault dip by considering three equally likely values of 45, 55, and 65 degrees.

Depth to the base of the seismogenic zone was based on depth distributions of seismicity in the region. Figure 6-4 shows east-west cross sections of the focal depth distribution of well located earthquakes (depth error < 2 km) in the region. The data indicate that most of the earthquakes occur shallower than about 18 km, with some as deep as 25 km. We consider the thickness of the seismogenic crust to be uncertain within the range of 15 to 20 km. The discrete probability distribution of 15 km [0.4], 18 km [0.4], and 20 km [0.2] is used to express this uncertainty. The depths of 15 and 18 km are favored because of the typical depth of large Basin and Range earthquakes and nearly all of the seismicity occurs shallower than 18 km.

Slip Rate

Fault slip rate provides a fundamental constraint on the average rate of seismic moment release and earthquake recurrence. Slip rate has the advantage of spanning a longer time period than the historical record, but there can be uncertainties both in measuring displacement and determining the ages of geologic units displaced. To the extent possible, estimated slip rates are based on published slip rates. Where reported rates are not available, slip rates (with wider uncertainty) are based on analogy with other mapped faults and/or by inferring the likely ages and amount of displacement based on reported descriptions of the faults.

Earthquake Recurrence Models

Earthquake recurrence is represented in terms of the rate of seismic activity and the relative frequency of various magnitude earthquakes. Earthquake recurrence for fault sources is assessed based on the slip rate on the fault as converted to seismic moment rate using fault area and from estimates of paleoseismic recurrence intervals when available.

The geologically derived seismic moment rate is used to translate slip rate into earthquake recurrence rate by partitioning the moment rate into earthquakes of various magnitudes according to a recurrence relationship (e.g., Anderson, 1979). Three general types of recurrence relationships have been proposed: (1) truncated exponential relations that mimic the behavior of recorded earthquakes in a region (e.g., Gutenberg and Richter, 1954); (2) a characteristic earthquake recurrence model (Youngs and Coppersmith, 1985) in which there is a greater tendency for earthquakes close to the maximum to occur than is predicted by seismicity-based exponential relations; and (3) relations that attribute all of the moment release on faults to earthquakes close to the maximum (Wesnousky, 1986). Each of these relationships were used in the probabilistic hazard analysis with relative weights of [0.22], [0.65], and [0.13] respectively. The assigned weights represent the average of the subjective judgements regarding the appropriate recurrence model for fault sources made by experts for the Yucca Mountain PSHA (CRWMS, 1998). The truncated exponential and characteristic magnitude distributions require a *b*-value to define the frequency of smaller earthquakes. The *b*-value obtained from the analysis of the regional seismicity (Section 6.2.2.1) was used for characterizing the earthquake recurrence models for the faults.

6.2.1.2 Fault Characterization

Sixteen fault sources are included in the seismic hazard analysis (Plate 6, Table 6-1, and Figure 6-3). The fault parameters used to characterize these sources are summarized in Table 6-2 and described below. Maximum magnitude distributions for individual fault sources are shown on Figure 6-6.

Mid-Valley Faults (Skull Valley)

Quaternary activity has been documented on a zone of faults within the southern Skull Valley that includes the East fault and the West fault. A similar fault, the postulated Springline fault has been inferred in the northern part of Skull Valley (Rigby, 1958; Hood and Wadell, 1968; Helm, 1995). Quaternary activity has not been documented for this fault, but based on analogy to the mid-valley faults in the southern part of the valley, the postulated Springline fault is assigned a probability of activity of 0.8 in this analysis. The East, West, and postulated Springline faults are collectively referred to as the mid-valley faults in this study. Alternative structural models (see Section 2.0 and Plate 6) that allow the possibility that some of these faults are linked or coalesce at depth, and could rupture together during individual earthquakes are considered for these fault sources. A logic tree summarizing the fault sources implied for each of these models is given in Figure 6-5.

The first node of the logic tree addressees the preference for the two alternative structural models presented in Section 2.0. These models chiefly reflect a difference in the assessment of the geometry and seismogenic capability of the West fault. In both models the East fault is included as active fault source that may, in some scenarios be linked along strike with the postulated Springline fault. Structural model A, in which the West fault splays from the East fault in the vicinity of Johnson Pass, best fits the available geologic and gravity data and thus, is given significantly more weight [0.8]. The alternative model B, which is given a weight of 0.2, allows for a longer West fault and captures the uncertainty in the southern extent of this fault.

Assessments of the seismogenic capability of the West fault are dependent on the structural model. In model A, the West fault may or may not be an independent seismic source depending on the geometry of the fault and possible intersection with the East fault at depth. Given the uncertainty in the geometries of these faults at depth, the probability of the West fault being an independent seismic source (i.e., it does not coalesce with the East fault above seismogenic depth) is assigned a weight of 0.5. In model B, the West fault is judged to be an independent fault source with a probability of 0.7. The higher weight given to the likelihood the fault is a seismic source is based on the structural relationships that require a fault between elevated bedrock in Hickman Knolls and the deep part of the basin, and evidence for late Pleistocene activity on the West fault. Lower weight [0.3] is given to the possibility that Hickman Knolls is a detached bedrock slide (i.e., is rootless), thus, obviating the need for a block-bounding fault to the west (see discussion in Section 4.4).

The second node of the logic tree addressees the likelihood that the East fault and the postulated Springline fault are linked along strike. A possible structural boundary between the northern and southern parts of Skull Valley is suggested by structural and gravity data. Helm (1995) noted that the Pass Canyon cross fault and a fault segment boundary along the Stansbury fault coincide with a regional alignment of tectonic features in the Oquirrh, Wasatch, and Uinta Mountains. The apparent truncation of Salt Mountain along this trend combined with gravity data that indicate the formation of two distinct depocenters in the northern and southern parts of the basin suggest that this structural trend persists across Skull Valley. This, in addition to the lack of geomorphic expression of continuity between the East and postulated Springline faults, is the basis for giving low weight [0.3] to the possibility the two faults are linked and higher weight [0.7] to the possibility they are independent fault sources.

Maximum rupture length scenarios for each of the proposed fault sources are summarized in Table 6-3. Postulated rupture segment boundaries are shown on Plate 6. Weights assigned to maximum rupture lengths (Table 6-2) reflect our judgment in the validity of the alternative segmentation models. The assessment of maximum magnitude distributions for the alternate fault sources are shown on Figure 6-6. These distributions reflect the postulated rupture dimensions based on combinations of rupture lengths and widths.

The slip rate distributions used for the individual fault sources (Table 6-2) vary depending on the structural model. Slip rate estimates for the East and West faults derived from paleoseismic data, which are discussed in Section 5.2, provide the basis for estimating the slip rate values used for the mid-valley faults. Generally, the highest weight is given to the central estimates, with less weight given to the end member values that capture the uncertainties in paleoseismic estimates. There is no independent slip rate data for the postulated Springline fault. In cases where the Springline fault is modeled as a separate source, it is given a slip rate distribution comparable to the East fault with weights more evenly distributed to reflect greater uncertainty. Slightly higher weight is given to higher slip rates in models in which the West fault coalesces with the East fault at depth and is treated as a single fault source (with or without linkage to the Springline fault).

Stansbury Fault

At its closest approach, the main trace of the Stansbury fault is 9 km west of the east border of the proposed PFSF site (Plate 6). The Stansbury fault dips to the west. A discussion of the nature and rate of Quaternary deformation on this fault is given in Section 5.1. The fault has a total length of 73 km, extending from the northern end of the Stansbury Mountains near the village of Timpie, to Lookout Pass at the southern end of the Onaqui Mountains (Plate 6). The fault sections identified by Helm (1995) are used herein with minor modifications. The fault sections include a 24-km-long section from Timpie south to Pass Canyon (Section "A"), and a 23-km-long section from Pass Canyon to Johnson Pass (Section "B"). In addition, we consider the possibility of additional fault sections south of Johnson Pass. The mapped fault trace and linear range front between Johnson Pass and The Dell, the substantial relief of the Onaqui Mountains, and the fault trace at the southern end of the range mapped by Sack (1993) all suggest the fault may continue to the south. We identify fault section "C", which extends from Johnson Pass to The Dell and is 9 km long. We also consider fault section "D", which extends from The Dell to Lookout Pass and is 17 km long (Plate 6).

We consider five rupture scenarios for the maximum-magnitude earthquake that incorporate various combinations of the four fault sections noted above. Because of the prominence of fault scarps across late Quaternary alluvial deposits along the Stansbury fault between Pass Canyon and Johnson Pass, as well as the proximity of this section, each of the scenarios includes rupture of section "B". The relatively short rupture of 23 km, in which section "B" ruptures alone, is given a low weight [0.1], because it is likely that the maximum earthquake includes rupture along at least one other section. Scenarios that include rupture of section "B" and an adjacent section are given higher probabilities, including a weight of 0.2 for the 47 km-long rupture of sections "A" and "B", and a weight of 0.3 for the 32-km-long rupture of sections "B" and "C". The 56-km-long scenario in which all three of the northern sections ("A", "B", and "C") rupture is weighted 0.3, based on the presence of evidence of recurrent displacement along all three sections. Lastly, the longest scenario, in which rupture occurs along all four sections of the entire 73-km-long fault, is weighted low [0.1] because of the discontinuity of the fault between The Dell and Lookout Pass.

The maximum magnitude distribution for the Stansbury fault (Figure 6-6) includes all five of the rupture scenarios and reflects the postulated rupture dimensions based on combinations of rupture lengths and widths. In addition, data for average displacement during a single event were included in the assessment. These data suggest that the average displacement during a single event on the segment of the Stansbury fault that lies closest to the site is between 2 to 3 m (see discussion in Section 5.1). As described in Section 5.1, the following distribution for average single event displacement was used in this analysis: 1 m [0.1], 2 m [0.4], 3 m [0.4], 4.5 m [0.1].

As discussed in Section 5.1, the estimated late Pleistocene slip rate of the Stansbury fault is in the range of 0.4 ± 0.1 mm/yr. We represent the uncertainty in slip rate with the discrete distribution of 0.3 mm/yr [0.2], 0.4 mm/yr [0.6], and 0.5 mm/yr [0.2].

East Cedar Mountains Fault

As part of a hydrologic reconnaissance of Skull Valley, Hood and Waddell (1968) inferred the presence of a fault having east-down displacement along the eastern margin of the Cedar Mountains. We informally refer to this fault as the East Cedar Mountains fault (Plates 6 and 7). This inferred fault extends from a point due east of Hastings Pass and about 7 km southwest of the village of Dell (along Highway 80), south along the eastern margin of the Cedar Mountains to the southern end of the range at the town of Dugway. At its closest location, the fault is 9 km from the proposed PFSF site. As shown by Hood and Waddell (1968), the fault contains a northern, 33-km-long section that strikes about N10°E, and a southern, 27-km-long section that strikes about N45°W. The total fault length as shown by Hood and Waddell (1968) is 60 km.

Later workers, concentrating on the presence of fault scarps present in alluvial deposits, did not acknowledge the existence of this fault (Everitt and Kaliser, 1980; Barnhard and Dodge, 1988;

Hecker, 1993). However, Arabasz and others (1989) included suspected Pleistocene fault scarps along the northeastern flank of the Cedar Mountains, north of the fault mapped by Hood and Waddell (1968), in their compilation of seismic sources in the region. These possible faults were based on photolineaments that had been identified, but not field checked, by Barnhard and Dodge (1988). Hecker (1993) designates these inferred faults as "Quaternary (?)" and shows them as a 10 km-long zone of short (<2 km) discontinuous fault scarps that are 2 to 3 km east of the range front. Considering these possible fault traces as part of the East Cedar Mountains fault, the fault extends from the northern end of the Cedar Mountains at Interstate 80, to the southern end of the range at the town of Dugway. This interpretation of the fault yields a total fault length of 72 km, with a 45-km-long northern section and a 27-km-long southern section.

The entire length of the East Cedar Mountains fault is within the area covered by the late Pleistocene Lake Bonneville, based on the location of the Bonneville and Provo shorelines mapped by Currey and others (1983), Barnhard and Dodge (1988), and Sack (1993). The possible fault traces at the northern end of the range mapped by Barnhard and Dodge (1988) are located basinward of the 10,000- to 11,000-year-old Gilbert shoreline shown by Sack (1993). This would suggest possible fault movement within the past 11 ka. However, detailed mapping of surficial deposits throughout Skull Valley by Sack (1993) does not show the presence of the possible fault identified by Barnhard and Dodge (1988). It is likely that the features identified by Barnhard and Dodge (1988) are not related to surface faulting.

In addition, Sack (1993) identified a 1.5-km-long, northeast-facing scarp along the eastern margin of the Cedar Mountains, approximately 9 km southwest of Hickman Knolls. This scarp also is basinward of the Provo shoreline and, if related to surface faulting, would suggest a surface-rupture earthquake within the past approximately 15,000 years. However, aerial reconnaissance and preliminary aerial photographic analysis conducted for the SAR submittal study showed no evidence of surface displacement at the location of the scarps noted by Sack (1993), nor anywhere else along the eastern Cedar Mountains range front between Rydalch Canyon and Dugway. Based on examination of aerial photography conducted for this study, the scarps identified by Sack (1993) are at the same elevation as sinuous lake shoreline features to the southwest and, thus may be shoreline rather than tectonic scarps.

We conclude that there is no definitive evidence of post-Bonneville displacement along the East Cedar Mountains fault, as implied by mapping by Everitt and Kaliser (1980), Barnhard and Dodge (1988), and Hecker (1993). However, with the available data, we cannot preclude the possibility of middle or late Pleistocene displacement (between 500 and 15 ka).

Based on the possible evidence for late Quaternary activity, the East Cedar Mountains fault is included as a fault source in the seismic source model for this analysis. We define the fault source to have a total length of 72 km, extending from the northern end of the Cedar Mountains at Interstate 80, to Dugway at the southern end of the Cedar Mountains (Plate 6). The East Cedar Mountains fault is assigned a probability of activity of 0.7 based on the questionable evidence of Quaternary activity and the possibility that this fault is truncated at depth by the west-dipping East fault at or above seismogenic depth. As shown on Figures 2-1 and 2-2, the overall basin geometry is consistent with a half graben bounded by the west-dipping East fault. The East Cedar Mountains fault, if it has been reactivated as a normal fault, may be truncated by the East fault at depths as shallow as 7 km. In the analysis the downdip width of the East Cedar Mountains fault incorporates the range of downdip extent permitted by varying fault geometries and dips for the East, West, and East Cedar Mountain faults.

We consider four possible values for the maximum rupture length, 12, 27, 45, and 72 km. A maximum rupture length of 12 km represents the average lengths of steep gradient segments that separate the more pronounced gravity anomalies. A maximum rupture length of 27 km represents the shortest straight segment of the fault that is well expressed as a linear gravity gradient. This length is comparable to the most well expressed segment of the Stansbury fault across Skull Valley. A maximum rupture length of 45 km represents the longest segment of the postulated fault. The lower three values of maximum length are given the most weight, 0.3, 0.4 and 0.15, respectively, because they are consistent with the overall structural framework of the valley and assessments of rupture lengths for the East and Stansbury faults. Rupture of the entire postulated length of the fault is given a weight of 0.05 because it is considered to be less likely than rupture of the entire Stansbury fault. No displacement data are reported for this fault. Therefore, the assessment of maximum magnitude is based empirical estimates of magnitude from assessments of rupture length and rupture area. The maximum magnitude distribution for the East Cedar Mountains fault, which reflects the postulated rupture dimensions based on combinations of the rupture length and width, is shown on Figure 6-6.

No slip rate data are available for the East Cedar Mountains fault. Assuming the East Cedar Mountains fault is an active fault, the slip rate probably is less than the slip rates for individual traces of the Stansbury fault, which are expressed as piedmont faults or the East fault. It is probably more analogous to the West fault, which is an intrabasin fault as opposed to the East fault, which bounds the Tertiary basin (half graben). Based on comparison to these faults and the lack or limited extent of late Pleistocene/Holocene scarps along the range front, the following slip rates and weights are used for the East Cedar Mountain fault: 0.01 mm/yr [0.25], 0.04 mm/yr [0.25], 0.07 mm/yr [0.25], 0.1 mm/yr [0.2], 0.45 mm/yr [0.05]. The weight is distributed relatively uniformly among the lower four values, which are considered equally likely, and significantly less weight is given to the highest value that is considered less likely given the lack of geomorphic expression of recent faulting.

Rush Valley Faults

A number of short discontinuous faults having Quaternary scarps have been identified along the western margin and in the central part of Rush Valley (Plate 7). These include the Clover fault, the Sheeprock fault, the Mid-valley Horst, and the Vernon Hills fault. As described below we consider alternate models for the zone of faults along the western margin of the valley. The relatively short (<7 km) faults that border the Mid-valley Horst and Vernon Hills that are more distant from the proposed PFSF site are not modeled as a specific fault sources.

Clover Fault

The Clover fault is a northwest-trending, east-dipping normal fault that borders the northeast flank of the Onaqui Mountains along the western margin of Rush Valley (Bucknam, 1977; Everitt and Kaliser, 1980; Hecker, 1993). This fault zone also is referred to as the North Onaqui East Marginal fault (Everitt and Kaliser, 1980; Krinitzsky, 1989). At its closest approach, the Clover fault zone is 27 km from the proposed PFSF site. Scarps in late Pleistocene to Holocene(?) alluvium indicate a minimum fault length of 4 to 7 km. The scarps have been modified by agricultural activities and, therefore, cannot be used to estimate the age of faulting. The graded profiles of streams that cross the fault suggest that the most recent faulting occurred more than several thousand years ago (Barnhard and Dodge, 1988). Arabasz and others (1989) assign an age of >15.5 ka to the timing of the last movement on this fault. Scarps heights of 1.1 to 1.2 m, and a single event displacement of 0.6 m, are reported for the Clover fault (Barnhard and Dodge, 1988; Krinitzsky, 1989).

The Clover fault is characterized as an active fault with a probability of 1.0. The total length of the Clover fault is uncertain. The fault is one of a series of short discontinuous zones of Quaternary faulting along the western margin of Rush Valleys. To the north, a short (1.3-km-long), east-facing fault scarp in older alluvium near East Hickman Canyon is mapped by Solomon (1993). To the south, Everitt and Kaliser (1980) identify lineaments and a possible scarp along the southeast flank of the Onaqui Mountains and prominent Quaternary fault scarps are mapped along the Sheeprock fault (Plate 7). The short lengths of these fault scarps suggest that the earthquakes that produced these scarps were at or near the threshold magnitude of surface rupture (i.e., M 6 to 6.5) and that the length of subsurface rupture may have exceeded the length of surface faulting. In order to address the uncertainty in the length and continuity of faults along the western margin of Rush Valley, alternate models and rupture scenarios for the Clover, East Hickman, and Sheeprock faults are considered.

Given the discontinuity of surface faulting along the western margin of Rush Valley and the evidence for a greater number of late Quaternary surface faulting events on the Sheeprock fault, relatively low weight [0.2] is given to a model (referred to as the west-side zone in Table 6-2) that allows for a continuous 52 km-long fault connecting the East Hickman Canyon scarp, Clover and Sheeprock faults. A maximum rupture length of 19 km [1.0] postulated for this fault zone reflects the lack of evidence for large magnitude earthquakes that would rupture the entire western margin zone.

Greater weight is afforded the model in which the Clover and Sheeprock faults are treated as independent fault sources. In this model the connection between the Clover fault and the fault scarps near Hickman Canyon is treated with uncertainty in the total length of the Clover fault. A weight of 0.25 is given to a total length of 7 km (the mapped length of the fault) and a weight of 0.75 is given to the combined length of 19 km.

The assessment of maximum magnitude is based on empirical estimates of magnitude from assessments of rupture length, rupture area, and single event displacement. It is uncertain whether the estimated single event displacement reported for this fault represents a maximum or average value. It is more likely that a single measurement along a fault represents the average value rather than the maximum, and thus the empirical relationship between maximum magnitude and average single event displacement is assigned higher weight [0.7] than the relationship based on maximum single event displacement [0.3]. The maximum magnitude distribution for the Clover fault is shown on Figure 6-6.

The slip rate for the Clover fault is not well constrained. The older alluvial fan deposits that are displaced by the Clover and East Hickman Canyon fault scarps are mapped as pre-Bonneville (>15.5 ka) (Everitt and Kaliser, 1980; Solomon, 1993). Based on scarp morphology the most recent episode of surface faulting appears to pre-date the Bonneville highstand and may be as young as ~35 ka on the East Hickman Canyon scarp (Solomon, 1993). Assuming that the older displaced alluvial fans are late Pleistocene (> 15.5 – 130 ka) and that only a single 0.6 m event has occurred along the Clover fault yields a slip rate of 0.004 to 0.04 mm/yr. Assuming that this event occurred ~35 ka yields a rate of 0.01-0.02 mm/yr. The small displacement and/or lack of multiple surface faulting earthquakes along this fault suggests relatively low rates of activity. Therefore, a slip rate distribution of 0.01 mm/yr [0.6] and 0.05 mm/yr [0.4] is assigned to the Clover fault (Model A). A slightly higher weight is assigned to the 0.05 mm/yr value in Model B (Clover and Sheeprock faults combined) based on the possibility of higher rates of activity on the Sheeprock fault.

Sheeprock Fault Zone

The Sheeprock fault is a northeast- to northwest-trending, east-dipping normal fault along the northeastern flanks of Sheeprock Mountain. At its closest approach, the Sheeprock fault is 41 km from the proposed PFSF site. A zone of Quaternary fault scarps extends about 10 to 11 km along the fault zone (Everitt and Kaliser, 1980; Barnhard and Dodge, 1988; Hecker, 1993; Bucknam, 1977). Scarp heights range from 1.9 to 16.5 m with some scarps representing repeated surface rupture (Barnhard and Dodge, 1988). A possible Holocene age was inferred for the most-recent event along the Sheeprock fault (Everitt and Kaliser, 1980). However, more recent scarp-profile investigations suggest that the Sheeprock scarps are older than the Topliff Hill and Mercur, which pre-date the Bonneville highstand (15.5 ka) (Barnhard and Dodge, 1988). Diffusion-equation modeling of the scarps yielded an age of about 53 ka for the scarps (Hanks and others, 1984). The embayed character of the range front suggests a long period of activity preceding the recent episode of faulting (Everitt and Kaliser, 1980).

The Sheeprock fault is characterized as active with a probability of 1.0. As discussed in the previous section a 0.8 probability is given to a model in which this fault is an independent fault source and a 0.2 probability that it is part of a more continuous fault that includes the Clover fault. The latter model is described in the previous section. Assuming that the Clover fault is an independent fault (Model A) we assume that the entire 18 km-long fault will rupture during a single earthquake. No displacement data are reported for this fault. Therefore, the assessment of maximum is based on empirical estimates of magnitude from assessments of rupture length and rupture area. The maximum magnitude distribution for the Sheeprock fault (Figure 6-6) reflects the postulated rupture dimensions based on combinations of the rupture length and width given in Table 6-2.

The slip rate for this fault is not well constrained. The higher fault scarps along this fault suggest a slightly higher level of activity relative to other Quaternary faults mapped within and along the western margin of the Tooele and Rush Valleys. The slip rate distribution used for this fault, 0.01 mm/yr [0.4], 0.05 mm/yr [0.5], and 0.1 mm/yr [0.1], is consistent with the rates estimated for faults within the valley and the more recently active structures (the Oquirrh, Mercur, Topliff Hill, and Stansbury faults) bounding the major ranges adjacent to the Tooele and Rush Valleys.

Oquirrh-East Great Salt Lake Fault Zone

The Oquirrh-East Great Salt Lake Fault Zone consists of a series of major westward-dipping, range-bounding Quaternary normal faults that includes the Oquirrh (Everitt and Kaliser, 1980; Olig and others, 1994) and East Great Salt Lake (Pechman and others, 1987; Viveiros, 1986) fault zones to the north and the East Tintic Mountain fault zones (Barnhard and Dodge, 1988) to the south (Plate 7). In their seismic hazard model, Youngs and others (1987) treat these faults as individual segments in a large fault zone they referred to as the Oquirrh Mountain fault zone, herein referred to as the Oquirrh-East Great Salt Lake fault zone. Each of these fault zones is described as a separate fault zone in the compilation by Hecker (1993). Wong and others (1995) present a segmentation model based on the following division of segments: the Promontory Mountains and Antelope Island segments of the East Great Salt Lake fault; the Oquirrh fault; the Mercur and Topliff Hill faults combined; and the East Tintic fault. In this analysis alternate models are considered that allow for both independent and dependent behavior of faults along this regional north-south trending zone of faults. Starting with the faults that lie closest to the proposed PFSF site, we discuss our segmentation model in the following sections.

Mercur-Topliff Hill Fault Zone

The Mercur-Topliff Hill fault zone consist of a zone of Quaternary faulting along the western side of the Oquirrh Mountains and Topliff Hill in Rush Valley (Plate 7). At its closest approach, this fault zone is 40 km from the proposed PFSF site. The Mercur fault zone consists of a 16-km-long alignment of late Pleistocene fault scarps along the western flank of the Oquirrh Mountain in Rush Valley. Based on exposures of faulted alluvium exposed in a mining shaft, together with an uplifted bedrock pediment, Everitt and Kaliser (1980) estimated a minimum of 60 m of Quaternary displacement on the fault. From scarp profile data, the Mercur scarps record displacements of 1.8 to 5.6 m (Barnhard and Dodge, 1988). Krinitzsky (1989) reports scarp heights of 2.1 to 7.7 m and a single event displacement of 0.9 to 1.9 m for the Mercur fault zone based on the scarp profile results of Barnhard and Dodge (1988). Solomon (1993) identified a small fault scarp south of the town of Stockton approximately 11 km north of the Mercur fault that exhibits a similar orientation and sense of displacement to the Mercur fault zone scarps. This scarp offsets late Pleistocene Lake Bonneville sediments, and it is not clear if it is related to surface-faulting events along the Oquirrh fault zone to the north or the Mercur fault zone to the south.

The Topliff Hill fault zone lies along the west flank of the northern East Tintic Mountains, a lower more subdued range to the south of the Oquirrh Mountain range (Hecker, 1993). A zone of fault scarps, which are relatively continuous for a distance of 12 km, exhibit a similar geomorphic position and sense of displacement as those along the Mercur fault zone. These scarps also show evidence for recurrent movement with a reported cumulative maximum displacement of 5.8 m; the scarps appear to be younger than the Mercur fault scarps based on scarp profile data (Barnhard and Dodge, 1988).

Everitt and Kaliser (1980) concluded that the most-recent surface faulting event along the Mercur-Topliff Hill fault zone post-dated the formation of the Bonneville shoreline. Barnhard and Dodge (1988) reinterpreted a trench log by Everitt and Kaliser (1980), and note that scarps along the Mercur-Topliff Hill fault zone are wave-etched and, therefore, are older than the Bonneville shoreline. Based on scarp morphology the Mercur-Topliff Hill fault zone scarps are interpreted to be late Pleistocene (Barnhard and Dodge, 1988; Hecker, 1993).

Based on the presence of scarps across and observed displacement of late Pleistocene deposits, the Mercur-Topliff Hill fault zone is included as a fault source with a probability of activity of 1.0. The continuity and relationship of the Mercur and Topliff fault zones in the subsurface is not known. Variations in the continuity, orientation, and possibly in the ages of the fault scarps along the zone of Quaternary faulting on the east side of Rush Valley suggest that these faults may behave as independent faults and this model (Model A) is given a weight of 0.4 in this analysis. A slightly higher weight is given to a model (Model B) in which these faults are considered to be part of the same fault zone. The shortest rupture lengths considered in both models reflect the length of relatively continuous fault scarps along both the Mercur and Topliff fault zones, 16 km and 12 km, respectively. A rupture length of 27 km for the Mercur fault zone is based on the assumption that the small fault scarp near Stockton is related to Mercur scarps. The 24- km-long postulated rupture length along the Topliff Hill fault zone assumes a rupture of both the southern linear range front segment and northern late Pleistocene segments of the Topliff Hill fault zone. The total length of the fault zone characterized in Model B is 56 km, the distance from Stockton to the southern end of the Topliff Hill fault zone. A 33 km-long rupture, equivalent to the combined length of late Quaternary faults scarps along the Mercur and Topliff Hill faults is given the most weight [0.5]. A shorter rupture length of 16 km, the length of the Mercur fault scarps and a longer rupture of the entire zone (56 km) are weighted 0.2 and 0.3, respectively.

The assessment of maximum magnitude is based on empirical estimates of magnitude from assessments of rupture length, rupture area, and single event displacement. It is uncertain whether the estimated single event displacement reported for this fault represents a maximum or average value. It is more likely that a single measurement along a fault represents the average value rather than the maximum, and thus the empirical relationship between maximum magnitude and average single event displacement is assigned higher weight [0.7] than the relationship based on maximum single event displacement [0.3]. The maximum magnitude distribution for both models (see Figure 6-6) reflects the postulated rupture dimensions based on combinations of rupture lengths and widths given in Table 6-2 and an estimated 0.9 to 1.9 m single-event displacement for the Mercur fault zone.

The slip rate on the Mercur and Topliff Hill fault zones is not well constrained. The assessed distribution for average slip rate shown in Table 6-2 was based on assumed ages for older alluvium displaced by the fault (Everitt and Kaliser, 1980) and comparison of these fault scarps to those along the Oquirrh fault zone. The estimated age of the soil developed on the older alluvium suggests that the alluvial fans along the flanks of the Oquirrh Mountains may be equivalent to Bull Lake alluvium estimated to be ~160 ka to 130 ka. Assuming that the 1.8- to 7.7-m-high scarps reflect net displacement post-130 ka and pre-14.5 ka suggests that the long-term average slip rate for the Mercur fault zone falls within the range of 0.01 to 0.5 mm/yr. A long-term slip rate of 0.03 mm/yr is estimated from the cumulative minimum Quaternary displacement of 60 m in ~1.8 Ma. The heights of the most recent fault scarps as well as the relative height of the adjacent ranges, suggests that the rate of slip along the Mercur and Topliff Hill fault zones is equal to or slightly less than Oquirrh fault zone, which is estimated to be 0.1 to 0.2 mm/yr (Olig and others, 1994). Slip rates of 0.1 to 0.2 mm/yr or less are typical of Basin and Range faults away from the Wasatch fault (Schwartz, 1987). Based on consideration of these estimates, a preferred range of slip rates and weights is used as follows: 0.05 mm/yr [0.5], 0.1 mm/yr [0.4], 0.2 mm/yr [0.1].

Oquirrh Fault Zone

The Oquirrh fault zone is a west-dipping normal fault that borders the western side of the Oquirrh Mountains in Tooele Valley. At its closest approach, the Oquirrh fault zone is 45 km from the proposed PFSF site. A variety of names have been used for this fault zone including: the Oquirrh marginal fault (Everitt and Kaliser, 1980); the northern Oquirrh fault zone

(Barnhard and Dodge, 1988; Hecker, 1993); and the Oquirrh fault zone (Olig and others, 1994). We follow Olig and others (1994) in referring to the zone of Quaternary faulting along the northern part of the Oquirrh Mountains as the Oquirrh fault zone. The fault zone extends for a least 21 km and has been subdivided into two sections: a northern section that includes fault scarps in alluvium, and a southern section that includes a fault contact between bedrock and alluvium along the range front (Everitt and Kaliser, 1980; Barnhard and Dodge, 1988). An additional segment near Silcox Canyon southwest of Tooele, identified by Everitt and Kaliser (1980) as a scarp of erosional or undetermined origin is identified by Solomon (1993) as a fault scarp. A zone of subsidiary faults lies within about 5 km west of the main fault in the southern Great Lake (Hecker, 1993). These faults may represent the northern extension of the Oquirrh fault zone.

Scarps along the Oquirrh fault zone range in height between 2.9 and 10.8 m, and surface offsets are between 1.3 and 7.3 m (Barnhard and Dodge, 1988). Locally, the compound scarps represent displacement during more than one surface-faulting earthquake. Scarps of the Oquirrh fault zone displace the Provo shoreline of Lake Bonneville. Studies of scarp morphology suggest that the most recent surface-faulting event occurred between 9 ka and 13.5 ka (Everitt and Kaliser, 1980; Barnhard and Dodge, 1988). More recently, paleoseismological investigations along the northern section of the Oquirrh fault zone by Olig and others (1994) documented that: (1) the most recent surface faulting event occurred between 4.3 ka and 6.9 ka, (2) the second-most-recent event occurred between 20.3 and 26.4 kyr B.P., (3) the net vertical tectonic displacement is between 1.9 and 3.3 m with best estimates of 2.2 and 2.7 m for the most-recent event and 2.3 m for the penultimate event, (4) the recurrence interval between the last two events ranges from 13.3 ka and 22.1 ka, (5) calculated slip rates are 0.1 to 0.2 mm/yr for this interval, and (6) the third-most-recent event probably occurred before 33.95 ± 1.16 ka.

Total length of the Oquirrh fault zone is estimated to be 35 km, which allows for the fault to extend a few kilometers northwards into the Great Salt Lake and includes the isolated, short, discontinuous fault scarps near Stockton. Comparison of the available information regarding timing of the surface-faulting events on the Oquirrh fault zone, and the Mercur fault zone to the south suggests that these fault zones have behaved as independent rupture segments since the Bonneville lake cycle (Olig and others, 1994). Available paleoseismic information is inconclusive regarding a possible rupture segment boundary between the Oquirrh fault zone and the East Great Salt Lake fault zone to the north (Olig and others, 1994). Wong and others (1995) summarize data that support a segmentation boundary in this area. Two rupture models, therefore, are considered: Model A, which treats the two latter faults as independent structures is given higher weight [0.9] based on data presented by Wong and others (1995) and Model B [0.1], which allows for ruptures to extend across the boundary between the mapped fault traces. A discussion of the offshore data used to evaluate this boundary is provided in the following section describing the East Great Salt Lake fault.

The rupture lengths and weights used in Model A are as follows: 12 km (the length of the northern section of the Oquirrh fault zone) [0.2]; 21 km (the combined length of the northern and southern sections) [0.4]; 35 km (the total length of the Oquirrh fault zone as described above) [0.4]. The rupture lengths and weights used in Model B reflect the possibility of longer ruptures due, in part, to the uncertainty in the continuity of fault segments that are mapped beneath the Great Salt Lake. Postulated rupture lengths for Model B are: 21 km [0.3], 35 km [0.5], and 52 km [0.2].

The assessment of maximum magnitude is based on assessments of rupture length, rupture area, and single-event displacement. The maximum magnitude distribution for both models (see Figure 6-6) reflects the postulated rupture dimensions based on combinations of rupture lengths and widths given in Table 6-2 and the estimated 2.2 to 2.7 m single event displacement for the Oquirrh fault zone. Olig and others (1994) note that the measured net vertical displacement values although limited in number are similar, suggesting they are closer to an average than an extreme. On this basis, we assume the 2.2 to 2.7 range reflects an average [0.7] rather than a maximum [0.3] single event displacement. As noted by Olig and others (1994), magnitude estimates based on displacement data are higher than those based on the 21 km length of the mapped fault.

Although recurrence data are available for the northern section of the Oquirrh fault zone, comparable data are not available for the rest of the Oquirrh fault zone or the East Great Salt Lake fault zone. Slip rate estimates are available for the Oquirrh fault zone as discussed above and for the East Great Salt Lake fault zone. These provide the basis for the estimated range of values given for both Models A and B in Table 6-2.

East Great Salt Lake Fault Zone

Gravity and seismic reflection data indicate that a major 100-km-long zone of faulting is concealed beneath the Great Salt Lake along the western margin of the NNW-trending linear topographic high that includes the Promontory Mountains, Fremont Island, and Antelope Island. This west-dipping fault, named the East Great Salt Lake fault zone by Cook and others

(1980), is clearly delineated in seismic reflection profiles across the lake (Mukulich and Smith, 1974; Smith and Bruhn, 1984; Viveiros, 1986; Pechmann and others, 1987; Mohapatra and others, 1993). These studies indicate that the fault exhibits normal displacement, generally strikes north-northwest and dips 30° to 50° to the west, and appears to have a listric geometry along at some of its length. At its closest approach, this fault zone is 66 km northeast of the proposed PFSF site.

This fault cuts sediments identified as Quaternary based on well data and appears to displace sediments within 10 to 20 m of the lake bottom (Viveiros, 1986; Hecker, 1993; Mukulich and Smith, 1974). A 1.5-km-long zone of *en echelon* fractures beneath the lake west of Antelope Island appears on aerial photos to have slight down-on-the-west displacement and to be unmodified by coastal processes, and thus may date from the latest Holocene (Smith and Bruhn, 1984; Hecker, 1993). Observations in drill holes suggest that the Mazama ash may be offset, inferring faulting may be younger than 6,800 yrs (D. R. Currey, written communication, 1994 as reported by Wong and others, 1995).

Following Pechmann (1987) and Wong and others (1995) we divide the East Great Salt Lake fault zone into two segments: a 40-km long Promontory Mountains segment and a 52 km- long Antelope Island segment. As noted above the relationship between the Oquirrh fault and the East Great Salt Lake fault zones is uncertain. Two rupture models as described in the previous discussion of the Oquirrh fault zone are considered: a model in which the two faults are independent fault sources (Model A) and a model in which ruptures may extend across the boundary between the two faults (Model B). In Model A rupture lengths postulated for the East Great Salt Lake fault zone are: 35 km (the length of the southern part of the fault zone bordered by Antelope Island), 40 km (the length of the northern segment), and 52 km (the length of the southern segment). In the combined rupture model (Model B) only the southern 52 km-long segment of the East Great Salt Lake fault zone is considered. The maximum magnitude distribution for both models (see Figure 6-6) reflects the postulated rupture dimensions based on combinations of rupture lengths and widths given in Table 6-2. The maximum magnitude distribution for Model B includes consideration of the paleoseismic evidence for single-event displacement outlined in Table 6-2.

Viveiros (1986) estimated fault slip rates on the East Great Salt Lake fault of 0.96 mm/yr during the Pliocene and 1.48 mm/yr during the Quaternary based on thickness of sedimentary deposits and inferred fault geometries. Vertical subsidence rates near the fault are estimated to be 0.3 to 0.5 mm/yr (Pechmann and others, 1987). Taking subsurface fault dip into account, these rates translate into fault slip rates of 0.4 to 0.7 mm/yr, assuming that the sedimentation rates are controlled by subsidence along the fault (Pechmann and others, 1987). These rates, which are approximately one-half of those measured for the Wasatch fault zone, are over double the rates estimated for the Oquirrh fault zone. Net tectonic displacements, however, may be considerably less than the measured subsidence due to antithetic faults and back-tiliting of the hanging wall. These possibilities are not discussed by Pechmann and others (1987). The distribution of estimated slip rates used for the East Great Salt Lake fault (Model A) and the combined East Great Salt Lake and Oquirrh fault zones (Model B) as listed in Table 6-2 incorporate the higher rates presented by Pechmann and others as well as the possibility that the rates are more comparable to those determined for the Oquirrh fault zone.

East Tintic Mountains Fault

The 36-km-long East Tintic Mountains fault is a north-trending, west-dipping fault along the western side of the East Tintic Mountains (Plate 7). At its closest approach, this fault is 72 km southeast of the proposed PFSF site. Isolated, highly dissected scarps in alluvium along the fault appear to be among the oldest in western Utah (Bucknam and Anderson, 1979). Anderson and Miller (1979) mapped buried Quaternary (?) faults extending to the north and south of the alluvial scarps. These faults and faults that form bedrock-alluvium contacts at the south end of the East Tintic Mountains (Morris, 1987) are mapped as Quaternary (?) by Hecker (1993). This fault zone was considered to be a segment of the Oquirrh fault zone as described by Youngs and others (1987). Given the differences in recency and activity along this fault compared with the Mercur-Topliff Hill, Oquirrh, and East Great Salt Lake fault zones to the north, we consider this fault as an independent fault source.

Postulated rupture scenarios allow for rupture of the entire (35 km) length of Quaternary faults along the western margin of the East Tintic Mountains as mapped by Hecker (1993), or rupture of the northern 20 km-long segment that includes the most recent scarps. These rupture lengths are given weights of 0.6 and 0.4, respectively. The assessment of maximum magnitude is based on empirical estimates of magnitude from assessments of rupture length and rupture area. The maximum magnitude distribution (see Figure 6-6) reflects the postulated rupture dimensions based on combinations of rupture lengths and widths given in Table 6-2. Given the lack of slip rate data, a slip rate distribution is estimated based on the lesser degree of activity of this fault as expressed geomorphically compared to the fault zones along trend to the north. The following range of slip rate values are used: 0.005 mm/yr [0.1], 0.01 mm/yr [0.4], 0.05 mm/yr [0.4], 0.1 mm/yr [0.1].

West Valley Fault Zone

The West Valley fault zone consists of a series of mostly east-dipping normal faults that displace late Quaternary lake deposits in Salt Lake Valley (Plate 7). At its closest approach, the West Valley fault zone is 75 km northeast of the proposed PFSF site. This fault zone was originally called the Jordan Valley fault zone and subsequently renamed the West Valley fault zone (Keaton and others, 1987). The southern portion of the fault zone consists of two subparallel east-facing scarps (the Granger and Taylorsville faults), whereas the northern portion is broader and is characterized by many smaller, east- and west-facing scarps. Locally, the near-surface expression of the fault zone is characterized by monoclinal flexuring and minor step-faulting. The total length of the zone is about 18 km (Keaton and others, 1987). Geomorphic and stratigraphic evidence of two events during the past 12 ka to 13 ka is documented along the main Granger and Taylorsville faults (Keaton and others, 1987). Geomorphic relations within the northern West Valley fault zone suggest that four or more events occurred in the same time period and that some of the post-Bonneville faulting occurred prior to formation of the Gilbert shoreline (12 ka). Borehole evidence associated with several traces of the northern West Valley fault zone suggests that the most recent event may have occurred 6 ka to 9 ka and that two or three events may have occurred since 22 ka to 28 ka (Hecker, 1993; Keaton and others, 1987). As noted by Youngs and others (1987), it is unclear whether movement on the West Valley fault zone is independent or directly tied to movement on the Salt Lake City segment of the Wasatch fault zone. A Holocene slip rate of 0.5 to 0.6 mm/yr is estimated for the Granger fault and the West Valley fault zone as a whole. Lower rates of 0.1 to 0.2 mm/yr are inferred for the Taylorsville fault over longer periods of time (< 140 ka). The relatively high slip rate calculated for post-Bonneville time suggests that strain release may be due to isostatic rebound within an extensional setting (Hecker, 1993).

The seismic source characterization used in this study follows that described in Youngs and others (1987). As noted by Youngs and others, it is unclear whether movement on the West Valley fault zone is independent or directly tied to movement on the Salt Lake City segment of the Wasatch fault zone. These two models are given weights of 0.6 and 0.4, respectively.

Given that the West Valley fault is an independently active source, it is modeled as a single fault segment because its overall length is so short. The maximum rupture length is assumed to be equal to the total length of the zone (18 km). The estimated slip rate distribution of 0.3 mm/yr [0.5], and 0.5 mm/yr [0.5] incorporates the range of available slip rate data.

Utah Lake Fault Zone

Latest Pleistocene to Holocene (?) faults and associated folds are identified over a 30 km length in Utah Lake based on seismic-reflection profile data (Brimhall and Merritt, 1981). At their closest approach, the Utah Lake faults are 79 km east of the proposed PFSF site (Plate 7). Due to the widely spaced seismic-reflection transects, the fault locations are uncertain. An 8- to 15-m-deep layer identified as the Provo Formation, which is interpreted to be lake bottom sediments probably deposited during the regressive phase of Lake Bonneville (Machette, 1989), is displaced from < 2 to 5 m across individual faults and folds beneath the lake. The reflection profiles suggest that displacements decrease upward in strata above this horizon and occur within several meters of the lake bottom.

It is not clear if movement on the Utah Lake fault zone is independent or directly tied to movement of the Wasatch fault zone. Based on the uncertainties in the geometries and tectonic significance of these structures, we assign the Utah Lake fault zone a probability of activity of 0.6 and treat it similar to the West Valley fault zone as discussed above. Rupture lengths of 20 km and 30 km, which reflect the lengths of the longer more continuous mapped traces and the total length of the fault zone, are assigned equal weight. The estimated slip rate distribution of 0.3 mm/yr [0.5], and 0.5 mm/yr [0.5] incorporates the range of available slip rate data.

Drum Mountains Fault Zone

The Drum Mountains fault zone is a series of north-trending, east-dipping faults along the eastern margin of the Drum Mountains. At its closest approach, the fault zone is 80 km south of the proposed PFSF site. Bucknam and Anderson (1979) map a 5-km-wide zone of fault scarps within pre-Lake Bonneville age deposits east of the Drum Mountains. The fault zone, as shown by Hecker (1993), is 36 km long. Faulted Provo-level shoreline features provide a maximum age of 13.5 ka for the scarps (Crone, 1983). Scarps range in height from 0.7 to 7.3 m, with average heights of 2.4 m, and show no geomorphic evidence of having multiple events (Hanks and others, 1984). Morphometric analyses of the scarps provide ages of 5.6 ka (Hanks and others 1984) and 9 ka (Pierce and Colman, 1986). Trenching by Crone (1983) showed that Holocene faulting produced 3.7 m of stratigraphic throw, significantly more than the 2.7 m of surface offset measured from nearby scarp profiles.

Based on the presence of scarps across and observed displacement of late Pleistocene deposits, the Drum Mountains fault zone is included as a fault source with a probability of activity of 1.0. A maximum rupture length of 36 km (the length of Holocene faulting) is assigned a weight of 1.0 based on the evidence for a single rupture event. The assessment of maximum magnitude is based on empirical estimates of magnitude from assessments of rupture length, rupture, area, and single-event displacement. The maximum magnitude distribution (see Figure 6-6) reflects the postulated rupture dimensions based on combinations of rupture length and widths and includes consideration of the paleoseismic evidence for single-event displacement as outlined in Table 6-2.

Based on the evidence of 3.7 m of slip in pre-Bonneville deposits reported by Crone (1983) and assuming an age range of ~30 ka to 160 ka for the pre-Bonneville deposits, the long-term slip rate for this fault ranges from 0.023 to 0.12 mm/yr. We use the following slip rate distribution in this analysis: 0.02 mm/yr [0.3], 0.05 mm/yr [0.4], and 0.2 mm/yr [0.3].

Fish Springs Fault

The Fish Springs fault is a north-trending, east-dipping fault along the eastern margin of the Fish Springs Range. At its closest approach, the fault is 81 km southwest of the proposed PFSF site (Plate 7). Bucknam and Anderson (1979) map the Fish Springs fault within alluvial fan deposits near the eastern base of the Fish Springs Range. The fault consists of a southern trace about 8 km long, and a northern fault trace about 3 km long. The potential fault rupture length, assuming scarps along both traces represent surface rupture in a single event, is about 12 km long (Bucknam and Anderson, 1979). A lack of scarp dissection and sharp nickpoints in small washes that cross the scarps suggest that the fault scarps are young (Bucknam and Anderson, 1979). The scarps occur below the level of the Bonneville shoreline and offset alluvial fan deposits that overlie shoreline features. The scarps therefore are younger than 12 ka. Field observations by Bucknam and Anderson (1979) suggest a maximum single-rupture surface offset of 3.3 m.

Based on the presence of scarps across and observed displacement of late Pleistocene deposits, the Fish Springs fault zone is included as a fault source with a probability of activity of 1.0. A maximum rupture length of 30 km (the length of the range front) is assigned a weight of 1.0. The assessment of maximum magnitude is based on empirical estimates of magnitude from assessments of rupture length, rupture, area, and displacement per event. The maximum magnitude distribution (see Figure 6-6) reflects the postulated rupture dimensions based on combinations of rupture length and widths given in Table 6-2 and an estimated 3.3 m maximum displacement per event for the Fish Springs fault. A long-term slip rate is not available for this fault. Based on analogy to the Drum Mountains fault zone and other low slip rate Basin and

Range faults, we use the following slip rate distribution in this analysis: 0.02 mm/yr [0.3], 0.05 mm/yr [0.4], and 0.2 mm/yr [0.3].

Wasatch Fault Zone

The 370-km-long Wasatch fault zone forms the eastern boundary of the Basin and Range province (Plate 1). The Wasatch fault zone contains nine westward-dipping normal fault segments that exhibit late Pleistocene or younger activity (Hecker, 1993). These segments are differentiated on the basis of timing of individual earthquakes and changes in scarp morphology and geometry (Machette and others, 1991). Three of the Holocene segments of the Wasatch fault zone are located within 100 km of the proposed PFSF site: the Salt Lake City, Provo, and Nephi segments. Paleoseismologic studies show that there have been repeated large-magnitude earthquakes on all three of these segments of the Wasatch fault zone. A seismic source model for the Wasatch fault zone is provided by Youngs and others (1987). The model was updated to incorporate current estimates of earthquake repeat times from McCalpin and Nishenko (1996), which reflect the results of paleoseismic studies conducted since 1987.

The 46-km-long Salt Lake City segment of the Wasatch fault zone is located approximately 81 km east of the proposed PFSF site. The Salt Lake City segment consists of three left-stepping surface traces that bound the western base of the Wasatch Range within Salt Lake City (Machette and others, 1991). The most-recent earthquake on the segment probably occurred 1,000 to 1,800 years ago (Hecker, 1993). However, diffusion-equation modeling of scarp degradation suggests a more recent age of 900 years. Based on Holocene fault scarps, average surface displacement per event is 2 m. Latest Quaternary slip rate estimates of 1 mm/yr are assigned to this segment of the Wasatch fault zone (Hecker, 1993).

Fault parameters used to characterize the Wasatch fault zone are presented on Table 6-2. Two models are considered: an unsegmented model and a segmented model. In the unsegmented model, the maximum rupture length is not constrained by the geologically defined segment boundaries and maximum rupture lengths up to 100 km are considered allowing for the simultaneous rupture of adjacent segments (Table 2 in Youngs and others, 1987). One hundred kilometers is about the maximum length of surface rupture reported for historic normal-faulting earthquakes (Wells and Coppersmith, 1994). Based on the results of paleoseismic investigations, which suggest the segments have ruptured independently during past earthquakes (Youngs and others, 1987; Machette and others, 1991), relatively low weight [0.2] is assigned to the unsegmented model compared to the segmented model [0.8].

Given the unsegmented model the average slip rate is judged to be in the range of 0.7 to 1.8 mm/yr based on the range of values reported by Hecker (1993) for the segments south of Collinston and north of Levan. The preferred value of about 1.1 mm/yr is based on the weighted average (weights were based on the relative segment lengths) of the central slip-rate values reported by Hecker (1993) for the Brigham City, Weber, Salt Lake City, Provo and Nephi segments. The range of values and assigned weights for the average slip rate on the Wasatch fault (unsegmented model) are: 0.7 mm/yr [0.05]; 0.9 mm/yr [0.2]; 1.1 mm/yr [0.4]; 1.3 mm/yr [0.25]; and 1.8 mm/yr [0.05].

Given the segmented model, the maximum rupture length for the each segment is taken as the total length of the geologically defined segments. The frequency of earthquakes is based on the recurrence data for past surface-faulting events compiled by McCalpin and Nishenko (1996) for each of the segments. McCalpin and Nishenko do not report recurrence intervals for the Collinston and Levan segments. These segments are at the north and south ends of the fault respectively. The end segments have a much lower rate of activity than the segments in between. Recurrence on these end segments was constrained using slip rate (Table 6-2). Based on 12-m high scarps in alluvium estimated to be several hundred thousand years old (Personius, 1990; Hecker, 1993), the slip rate on the Collinston segment is significantly lower than along the segment to the south. The actual rate is not well constrained. The following range of values was included in the hazard analysis: 0.02 mm/yr [0.45]; 0.04 mm/yr [0.45]; and 0.08 mm/yr [0.1]. The slip rate on the Levan segment also is not well constrained. Based on a single Holocene event (Jackson, 1991), the slip rate on the Levan segment is estimated to be <0.3 mm/yr (Hecker, 1993). The range of values included in the hazard analysis is: 0.05 mm/yr [0.1]; 0.1 mm/yr [0.4]; 0.2 mm/yr [0.4]; and 0.3 mm/yr [0.1]

6.2.2 Seismic Source Zones

Four areal source zones as shown on Figure 6-7 are incorporated into the seismic hazard model for this study. The Wasatch fault zone forms the boundary between the central and eastern zones. The boundaries between the central and western zones are defined by the apparent change in the number of recorded earthquakes in the three areas. The southeastern corner of the eastern source zone was configured to exclude the areas of coal mining induced seismicity defined by Arabasz and others (1997).

6.2.2.1 Recurrence

The earthquake catalog used in this study was compiled by the University of Utah. The catalog includes both the historical and instrumental earthquake records, which extend from 1850 to

July, 1962 and July, 1962 to the present, respectively. The historical period begins with the first publication of a Utah newspaper in 1850 and has been carefully cross-checked and annotated with several sources of information, including the NOAA earthquake data file at the National Geophysical Data Center, by the University of Utah. The instrumental period of the catalog relies heavily on the University of Utah network data. The instrumental record begins in July of 1962 with data recorded from 26 stations statewide, with improvements in coverage and instrumentation occurring in 1974 and 1981. A comprehensive documentation of the catalog is given in Arabasz and others (1989), which was created for the proposed siting of the Superconducting Super Collider (SSC). The catalog was upgraded significantly for the SSC project, including deletion of quarry blasts and duplicate recordings of events, and modification of magnitudes to make them consistent between different networks and historical recordings, thus making further improvement of the catalog unnecessary for this project. We incorporated the preliminary estimates of M_L for events past 1994 (W. Arabasz, personal communication, 1999).

For this project seismicity data were pulled for an approximately 200-km radius region encompassing the site (Figure 6-7). The maximum recorded magnitude in the region shown on Figure 6-7 is a **M** 6 event (10/6/1909). Seismic activity for the region is depicted on Figure 6-7 along with the regional source zones. The pattern of seismicity is fairly evenly distributed along the Wasatch Range, with clusters of activity occurring to the west and east of the range.

The estimation of earthquake recurrence parameters requires the identification and removal of dependent events (foreshocks and after shocks) and specification of the periods of complete reporting. Dependent events were identified using the methodology described by Youngs and others (1987).

Estimation of recurrence parameters also requires an assessment of the time period over which there has been complete reporting of earthquakes (see Stepp, 1972). Youngs and others (1987) analyzed the earthquake catalog for north-central Utah and found the following periods of catalog completeness:

Magnitude Range	Period of Complete Reporting
3.0 - 4.0	10/01/1974 to present
4.0 – 5.3	01/01/1938 to present
5.3 – 6.0	01/01/1875 to present
>6.0	01/01/1850 to present

The above periods of compete catalog reporting were used to estimate the recurrence parameters for each of the seismic source zones using the maximum likelihood technique (Weichart, 1980). Figure 6-8 shows the resulting recurrence relationships compared to the recorded seismicity within each source zone. The uncertainty in the recurrence relationship for each source zone was modeled by specifying a range of possible *b*-values and seismicity rates and computing the relative likelihood that each to the resulting recurrence relationships generated the observed earthquake catalog. These relative likelihoods were normalized into discrete probability distributions for the recurrence parameters (see Figure 6-3).

6.2.2.2 Maximum Magnitude

Most of the large earthquakes that have occurred in the Basin and Range province can be associated with specific faults. For this assessment, we assess the maximum size of an earthquake that might occur on an unrecognizable fault and use this to assign maximum magnitudes to the seismic source zones. Because the hypothesized fault is unrecognized from surface geologic studies, its maximum magnitude is considered to be the largest earthquake that can occur without rupturing the surface (termed the threshold of surface faulting). Wells and Coppersmith (1993) have studied the presence or absence of surface faulting as a function of magnitude. Their studies have shown that the magnitude at which there is a 50% probability of surface faulting is magnitude 6; at magnitude 5.5 the probability is about 20% and at magnitude 6.5 the probability is about 80%. Based on these analyses, we consider the maximum magnitude for an earthquake occurring in the seismic source zones to be uniformly distributed in the range of **M** 5.5 to 6.5, with a mean value of 6.0.

6.3 GROUND MOTION ATTENUATION MODELS

At present, strong motion data recorded in Utah are very limited. In the past, evaluations of seismic hazard, (e.g., Youngs and others, 1987) have typically concluded from examination of the limited strong and weak motion (i.e. seismographic network recordings) that strong ground motion attenuation relationships developed from analysis of California earthquake recordings can be used for Basin and Range sites. However, more recent studies have used examinations of world-wide normal faulting earthquake data together with a variety of modeling techniques to infer that there may be significant differences between strong ground motions in California and those from normal faulting earthquakes in extensional tectonic regimes, such as the Basin and Range region of north-central Utah. Much of this work was reviewed as part of the seismic hazard assessment for the proposed nuclear waste repository at Yucca Mountain, Nevada (CRWMS M&O, 1998). As part of that study, a panel of seven ground motion experts was assembled to provide assessments of the appropriate ground motion models for the Basin and

Range region of southern Nevada. In that study, two basic approaches were used to develop ground motion attenuation relationships, one based on modifications to empirical California strong motion attenuation relationships and one based on numerical modeling. For this study, we utilize results of the Yucca mountain study to adapt California empirical ground motions to the conditions at Skull Valley, Utah. The modifications to the empirical attenuation relationships account for the effects of the characteristics of the earthquake source, the crustal wave propagation path, and the local site geology. The results of the numerical modeling conducted for Yucca Mountain are site-specific to the conditions there and are not directly transferable to the Skull Valley site. Therefore, they were not used in this study.

Appendix F describes the selection and modification of the empirical attenuation models for this study. The Yucca Mountain Ground Motion Expert Panel selected seven empirical ground motion attenuation relationships for modeling rock site motions from normal faulting earthquakes. As discussed in Appendix F, six these were selected to assess horizontal ground motions at the Skull Valley site. These are: Abrahamson and Silva (1997), Boore and others (1997), Campbell (1997), Idriss (1997), Sadigh and others (1997), and Spudich and others (1997). The relationships developed by Abrahamson and Silva (1997), Campbell (1997), and Sadigh and others (1997) also provide assessments of vertical ground motions.

With the exception of the Spudich and others (1997) model, the selected empirical attenuation relationships were developed primarily from California strike-slip and reverse faulting earthquake data. The Yucca Mountain Ground Motion Expert Panel developed five alternative sets of scaling factors to adjust these relationships to normal faulting conditions. For this study we adopted these scaling factors, resulting in twenty alternative attenuation relationships for horizontal motions and eleven for vertical motions. We also adopted the averages of the relative weights assigned to these factors by the seven panel members (see Tables F-1 and F-2).

Following the approach used by the Yucca Mountain Ground Motion Expert Panel, we also adjust the selected attenuation relationships for the lower rate of ground motion attenuation (higher Q) in north-central Utah as compared to California, and for the expected difference in the response of the Skull Valley sediments compared to the California alluvial soils represented in the empirical data used to derive the attenuation relationships. These adjustments are described in Appendix F.

Two alternative site adjustment factors are developed in Appendix F to adjust the rock site attenuation relationships to the subsurface conditions at the Skull Valley site. The first is based on site response modeling. The response of the Skull Valley profile is compared to the response of profiles appropriate to the rock site attenuation relationships. The second is based on comparing empirical strong motion data recorded on shallow soil sites (the conditions at Skull Valley) to ground motion levels predicted using the rock site attenuation relationships. As discussed in Appendix F, the site adjustment factors based on the site response model are given twice the weight assigned to the empirical site adjustment factors (0.67 versus 0.33 weight).

Figure 6-9 compares the resulting attenuation relationships for horizontal ground motions. Shown on the plots are the estimated ground motions for peak ground acceleration and 5%-damped spectral acceleration at a period of 1.0 second. Each of the six attenuation relationships is shown with the multiple scaling factors for seismic source effects and the two alternative site adjustment factors. Figure 6-10 presents similar comparisons for the vertical attenuation relationships.

6.4 PROBABILISTIC SEISMIC HAZARD RESULTS FOR GROUND SHAKING HAZARD

Seismic hazard calculations were made for peak ground acceleration and 5%-damped response spectral accelerations at periods of 0.075, 0.1, 0.2, 0.3, 0.5, 1.0, 2.0, and 4.0 seconds for horizontal and vertical motions. For hazard computations, the fault-specific sources were modeled as segmented planar surfaces. The areal source zones were modeled as a set of closely spaced parallel fault planes occupying the source regions outlined in Figure 6-7. The probability density function for distance to earthquake rupture for each source was computed assuming earthquake ruptures were uniformly distributed along the length of the fault plane. The depth distribution for earthquakes was based on the observed depth distribution for well-located earthquakes shown on Figure 6-4. The distance density functions were computed consistent with the distance measure used in each of the attenuation relationships. A rectangular rupture area for a given size earthquake is located at a random point on the fault plane. The closest distance to this rectangle was used as the distance measure in the Abrahamson and Silva (1997), Idriss (1997), and Sadigh and others (1997) models. The same distance was used in the Campbell (1997) model, except that the rupture was not allowed to come shallower than two km. For the Boore and others (1997) and Spudich and others (1997) relationships, the rectangular rupture area on the fault was projected vertically to the surface and the closest distance to this surface projection was used.

The rupture size of an event was specified by the relationship $\ln(\text{area}) = 2.095\mathbf{M} - 7.88$ developed from the results presented in Wells and Coppersmith (1994). The specified relationship gives the mean rupture area for a specific magnitude rather than the median (mean log) rupture area. Studies by Bender (1984) have shown that the use of mean estimates of rupture size in the computation of hazard yields results nearly equal to those obtained when the statistical uncertainty in the size of individual ruptures is incorporated in the analysis. The hazard was computed with the distribution in peak ground motion above the median attenuation relationships truncated at three standard deviations.

Distributions for the annual frequency of exceeding various levels of peak ground acceleration and spectral acceleration were developed by performing hazard computations using Equation (6-2) with the input parameters defined by each end branch of the logic trees. The hazard was computed considering the contributions of earthquakes of magnitude **M** 5 and larger (m^0=5). At each ground motion level, the complete set of results forms a discrete distribution for frequency of exceedance, $\nu(z)$. The computed distributions were used to obtain the mean frequency of exceeding various levels of peak ground motion (mean hazard curve) as well as hazard curves representing various percentiles of the distributions. The logic trees represent our best judgement as to the uncertainty in defining the input parameters and thus the computed distributions represent our confidence in the estimated hazard.

6.4.1 Computed Hazard for Horizontal Ground Motions

Figure 6-11 presents the computed mean peak hazard and the 5th- to 95th-percentile hazard curves for peak horizontal acceleration and 5%-damped horizontal spectral acceleration at a period of 1.0 second at the CTB site. The uncertainty band is about ¾ of an order of magnitude in frequency of exceedance at low ground motion levels to an order of magnitude at large ground motion levels. The distribution in computed frequency of exceedance is somewhat skewed with the mean frequency of exceedance lying above the median.

Figure 6-12 shows the contributions of the various seismic sources to the total hazard. The dominating sources are the Stansbury and the East-Springline faults. The relative contribution of the Stansbury fault increases for long period ground motions because of the potential for the occurrence of larger earthquakes on this fault compared to the Skull Valley faults (see Figure 6-6).

Figure 6-13 shows the relative contribution of events in different magnitude intervals to the computed mean hazard. Each plot in the figure presents a histogram of the percent contributions of events in 0.25 magnitude unit-wide intervals separated by distance from the site. Histograms are presented for peak acceleration and spectral acceleration at a period of 1.0 seconds for mean annual frequencies of exceedance of 2×10^{-3}, 5×10^{-4}, and 10^{-4} (return periods of 500, 2,000 and 10,000 years, respectively). The hazard is dominated by ground motions from nearby **M** 6 to 7 events, consistent with the dominance of the Stansbury and East-Springline faults.

The distributions in the computed hazard shown on Figure 6-11 represent the cumulative effect of all levels of parameter uncertainty included in the hazard model logic trees. The relative contribution of various components of the model to the overall uncertainty can be readily identified from the logic tree formulation. This is accomplished by selecting the node for the parameter to be examined and then computing the hazard, giving each branch in succession a weight of unity and all other branches at that node zero weight. For example, the contribution of uncertainty in selecting the appropriate attenuation relationship can be obtained by computing the mean hazard assuming each of the five attenuation relationships is, in turn, the "correct" relationship, with weight of 1.0, and the other five have zero weight. The resulting hazard curves are shown on Figure 6-14. In the plots, the heavy solid curve corresponds to the mean hazard and the light solid curves the 5th- and 95th-percentiles of the distribution in exceedance frequency from Figure 6-11. The six labeled curves are the resulting conditional mean hazard for each of the attenuation relationships. These are then mean results over the alternative source scaling relationships applied to each attenuation relationship (see Appendix F, Table F-1). The difference between the conditional means represent the uncertainty in the computed hazard due to uncertainty in selecting the appropriate attenuation relationship. The results shown on Figure 6-14 indicate that the choice of attenuation relationship is a major contributor to uncertainty in the hazard.

Figures 6-15 and 6-16 show the effect of the alternative scaling factors applied to the empirical attenuation relationships on the computed hazard. Figure 6-15 shows the effect of the alternative source scaling factors on the hazard. It is expected that the "Q only" scaling would produce the highest hazard. However, for peak ground acceleration, the highest hazard results from the use of the Abrahamson and Silva (1997) attenuation relationship (Figure 6-14). The Yucca Mountain Ground Motion Expert Panel did not apply "Q only" scaling to this relationship. Thus the "Q only" scaling curves shown on Figure 6-15 are the weighted combination of the other five attenuation relationships with "Q only" scaling applied. If "Q only" scaling had been applied to the Abrahamson and Silva (1997) relationship, then the combined "Q only" scaling result would have been noticeably higher.

Figure 6-16 shows the effect of the alternative site adjustment factors on the computed hazard. There is a significant effect on the peak acceleration hazard reflecting the significant difference in the two site adjustment factors defined in Appendix F. A low frequencies the two approaches yield similar site adjustment factors, and thus similar hazard levels.

Figures 6-17, 6-18, and 6-19 show the effect of the alternative modeling of the Skull Valley faults (see Figure 6-5) on the hazard computed from these sources alone (the contribution from the other sources shown on Figure 6-12 is not included). Figure 6-17 shows the effect of the alternative models for the geometry and extent of the West fault. As can be seen from the figure, the alternative models have little effect on the hazard. This is because the East fault dominates the hazard from the Skull Valley faults due to its higher assessed slip rate (see Figure 6-12) and the alternative models for the West fault have only a minor effect on the parameters for the East fault. Similarly, Figure 6-18 shows that consideration of the West fault as an independent source or as a secondary feature for the west fault has a minimal impact on the hazard. Figure 6-19 shows the effect of considering the East and Springline faults to be separate segments or to be linked into a single fault. Considering them to be combined into a single fault produces slightly higher hazard at low probabilities of exceedance and for longer period motions because of the potential for large magnitude earthquakes to occur on the combined source than when they are considered to be separate segments.

Figure 6-20 compares the computed hazard in the western portion of the site area to the hazard at the CTB building. The hazard at the two locations is nearly identical.

6.4.2 Computed Hazard for Vertical Ground Motions

Figure 6-21 presents the computed mean peak hazard and the 5^{th}- to 95^{th}-percentile hazard curves for peak vertical acceleration and 5%-damped vertical spectral acceleration at a period of 1.0 second at the CTB site. The uncertainty band for vertical peak acceleration hazard is similar to that obtained for horizontal peak acceleration, while the uncertainty for vertical spectral acceleration hazard at a period of 1.0 second is somewhat smaller that that obtained for horizontal spectral accelerations.

Figure 6-22 shows the contributions of the various seismic sources to the total hazard for vertical motions. As was the case for horizontal motions, the dominating sources are the Stansbury and the East-Springline faults.

Figure 6-23 shows the effect of the alternative attenuation relationships on the mean hazard for vertical motions. There is greater spread in the hazard results for peak vertical acceleration than for vertical spectral acceleration because the vertical spectral acceleration attenuation relationships produce more similar estimates than the vertical peak acceleration attenuation relationships at close distances (see Figure 6-10).

6.4.3 Contributions to Uncertainty

Figure 6-24 summarizes the contributions to the uncertainty in the total hazard at the CTB site. The plots present histograms showing the relative contribution of the various components of the uncertainty model (logic trees) to the uncertainty in the total hazard at ground motion levels corresponding to a return period of 2,000 years. The components are listed across the bottom and are in order: site adjustment factor (WUS rock to Skull Valley), empirical attenuation model, earthquake source scaling factor (California strike-slip to normal faulting), maximum seismogenic depth of faulting, alternative models for the West fault geometry, independence of the West fault, fault segmentation, fault activity, fault dip, maximum magnitude, seismic source recurrence rate, *b*-value of exponential portions of recurrence relationships, and magnitude distribution model. The major contributors to the uncertainty in the hazard are the selection of the alternative attenuation relationships, selection of the approach to the site adjustment factor, and assessment of maximum magnitude, recurrence rate and form of the magnitude distribution for the faults.

6.4.4 2,000-yr Equal-hazard Spectra

Figure 6-25 shows the mean hazard curves for peak ground acceleration and 5%-damped spectral acceleration at eight spectral periods for horizontal and vertical motions. These hazard curves were interpolated to obtain ground motions with a return period of 2,000 years (annual frequency of exceedance of 5×10^{-4}). Figure 6-26 compares the resulting equal-hazard spectra for horizontal and vertical motions. The spectral accelerations are listed in Table 6-4.

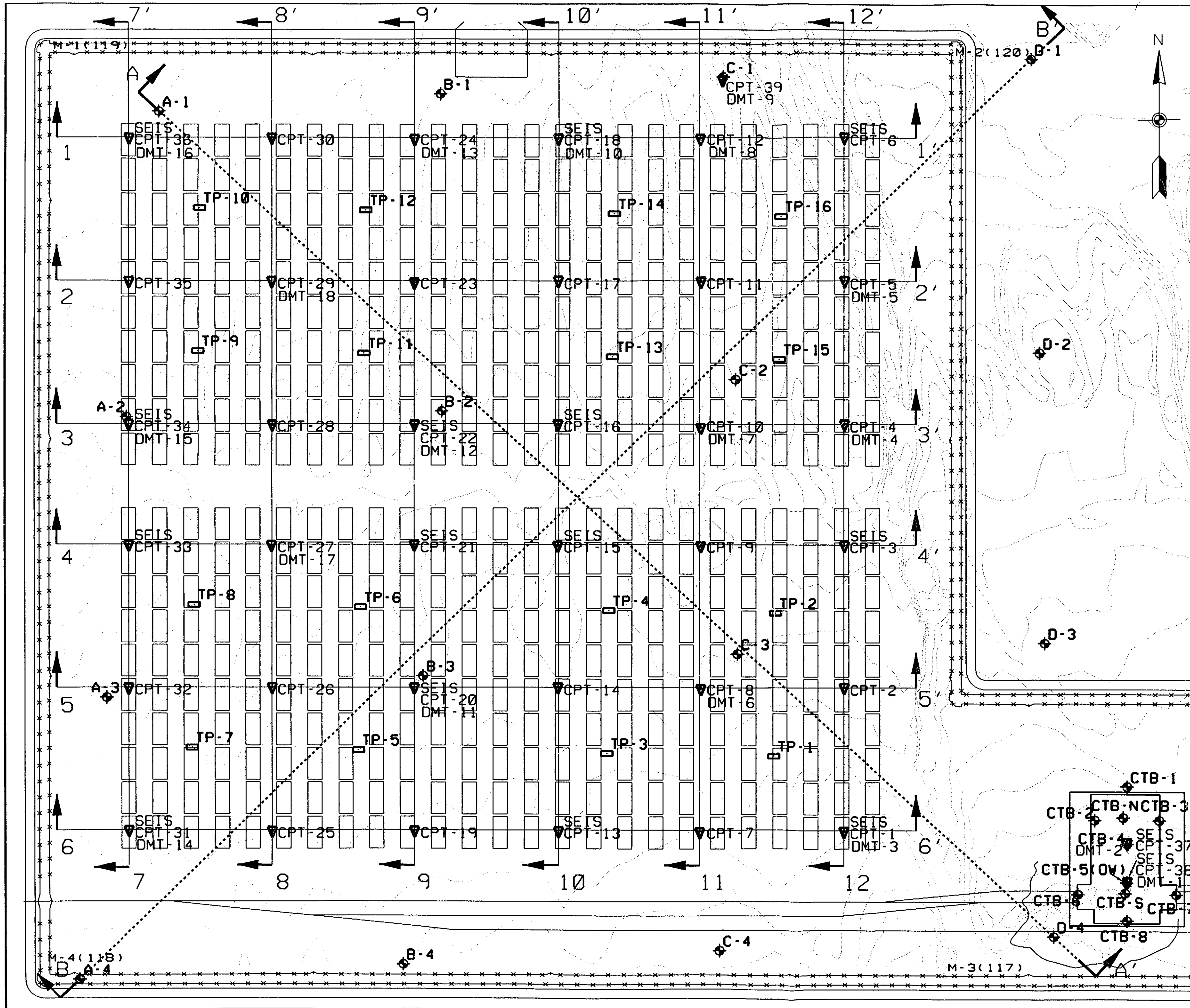

LEGEND:

CPT-1 DMT-3 ▼ CONE PENETRATION TESTS AND DILATOMETER TESTS

C-3 ⯐ STONE & WEBSTER BORINGS

M-4(118) ▲ SURVEY CONTROL POINT

TP-1 ▭ TEST PIT

0 200 400 FEET

1" = 200'-0"

FIGURE 2.6-19

LOCATIONS OF CONE PENETRATION, TEST PIT AND DILATOMETER TESTS

PRIVATE FUEL STORAGE FACILITY
SAFETY ANALYSIS REPORT

\site\fig-2 6-19-sar.dgn May. 17, 2001 08:01:39